Journal of Applied Physics

Controlled doping of graphene by impurity charge compensation via a polarized ferroelectric polymer

Cite as: J. Appl. Phys. **127**, 125503 (2020); https://doi.org/10.1063/5.0003099
Submitted: 30 January 2020 . Accepted: 11 March 2020 . Published Online: 24 March 2020

Kelotchi S. Figueroa, Nicholas J. Pinto, Srinivas V. Mandyam, Meng-Qiang Zhao, Chengyu Wen, Paul Masih Das, Zhaoli Gao, Marija Drndić, and A. T. Charlie Johnson

Journal of Applied Physics ARTICLE scitation.org/journal/jap

Controlled doping of graphene by impurity charge compensation via a polarized ferroelectric polymer

Cite as: J. Appl. Phys. **127**, 125503 (2020); doi: 10.1063/5.0003099
Submitted: 30 January 2020 · Accepted: 11 March 2020 ·
Published Online: 24 March 2020

View Online Export Citation CrossMark

Kelotchi S. Figueroa,[1] Nicholas J. Pinto,[1,a)] Srinivas V. Mandyam,[2] Meng-Qiang Zhao,[2] Chengyu Wen,[2] Paul Masih Das,[2] Zhaoli Gao,[2,b)] Marija Drndić,[2] and A. T. Charlie Johnson[2]

AFFILIATIONS

[1]Department of Physics and Electronics, University of Puerto Rico at Humacao, Humacao 00791, Puerto Rico
[2]Department of Physics and Astronomy, University of Pennsylvania, Philadelphia, Pennsylvania 19104, USA

[a)]**Author to whom correspondence should be addressed:** nicholas.pinto@upr.edu
[b)]**Present address:** Department of Biomedical Engineering, Chinese University of Hong Kong, Hong Kong.

ABSTRACT

A simple technique of doping graphene by manipulating adsorbed impurity charges is presented. Using a field effect transistor configuration, controlled polarization of a ferroelectric polymer gate is used to compensate and neutralize charges of one type. The uncompensated charges of the opposite type then dope graphene. Both *n*- and *p*-type doping are possible by this method, which is non-destructive and reversible. We observe a change in *n*-type dopant concentration of 8×10^{12} cm^{-2} and a change in electron mobility of 650%. The electron and hole mobilities are inversely proportional to the impurity concentration, as predicted by theory. Selective doping of graphene can be achieved using this method by patterning gate electrodes at strategic locations and programming them independently. Such charge control without introducing hard junctions, therefore, permits seamless integration of multiple devices on a continuous graphene film.

I. INTRODUCTION

Graphene is a two-dimensional solid consisting of planar sp^2-bonded C atoms arranged in a honeycomb lattice.[1] The valence and conduction bands meet at a point for monolayer graphene, which is known to exhibit an ambipolar electric field effect.[2–4] Since semiconductor devices rely on both *p*- and *n*-type conduction during operation, graphene based electronics are conceivable if their electrical properties can be manipulated. Chemical doping is one way to accomplish this via carbon substitution[5,6] or via charge transfer between adsorbed dopants and the graphene surface.[7–10] Substitution disrupts ideal sp^2 hybridization of carbon atoms,[5,6,11,12] while chemisorption of dopants and their subsequent reaction with other adsorbates leads to irreversible doping effects.[10] Both these outcomes are undesirable.

We report a simple technique to dope graphene by taking advantage of the impurity charges adsorbed on its surface during fabrication and by using the polarization of a ferroelectric (FE) polymer gate in a field effect transistor (FET) configuration. This technique is non-destructive and reversible. There is no charge transfer between the FE polymer and graphene, but there is basically field effect doping, similar to the "chemical gating" mechanism of graphene sensors.[8] By programming the rate at which the gate voltage is increased or decreased, the magnitude and direction of polarization (↓ or ↑) can be controlled. This results in *n*- or *p*-type doping in graphene. A polarized FE gate compensates and neutralizes one sign of impurity charges that were unintentionally adsorbed on to the graphene surface during fabrication. Doping then originates from the uncompensated impurity charges of the opposite sign on the graphene surface. The electron and hole mobilities changed by 650% and 200%, respectively, while the change in *n*-type dopant concentration approached 8×10^{12} cm^{-2} for electrons. Selective doping of graphene can be achieved using this method by patterning gate electrodes at strategic locations and programming them independently. Such charge control without introducing hard junctions, therefore, permits seamless integration of multiple devices on a continuous graphene film. Retention of the

polarized state in the absence of a gate voltage also extends its use in conjunction with other finite bandgap 2D materials, to applications ranging from high performance photodetectors, non-volatile memory transistors, diodes, and logic devices.[13–16]

II. EXPERIMENTAL

Monolayer graphene was grown via chemical vapor deposition (CVD)[17] and transferred on to a pre-patterned Si^{+}/SiO_2 substrate (see the supplementary material). Figure 1(a) shows an atomic force microscope (AFM) image of a CVD grown graphene film used in this work, and Fig. 1(b) shows the Raman spectrum with a symmetric 2D band at ~2670 cm^{-1} and a bandwidth of ~30 cm^{-1}. The AFM height profile and location of the G and 2D bands are characteristic features of monolayer graphene.[18] Transmission electron microscopy–selected area electron diffraction (TEM–SAED) data also confirm that the graphene used is one layer thick (see Fig. S1 in the supplementary material). A thin film (200 nm) of the ferroelectric copolymer poly(vinylidene fluoride–trifluoroethylene) (PVDF–TrFE) (75/25)[19] was spun coated from a 9 wt. % solution in N-methylpyrrolidinone (NMP) and air dried for 24 h at 70 °C. A higher annealing temperature was avoided to reduce the possibility of gate leakage currents. Using an Al foil as a shadow mask, Ag was thermally evaporated over the PVDF–TrFE coated graphene. Electrical measurements were carried out under a vacuum of 10^{-2} Torr. Figure 1(c) shows the schematic of the device, and Fig. 1(d) shows an optical image of the actual device. Two adjacent Au fingers form the source (S) and drain (D) terminals, while contact on Ag forms the gate terminal (G) of the graphene ferroelectric field effect transistor (FE-FET). The channel length and width of the device were 3 μm and 145 μm, respectively (see Fig. S2 in the supplementary material for experimental details).

III. RESULTS AND DISCUSSION

Figure 2 shows the drain-source current (I_{DS}) vs gate-source voltage (V_{GS}) of the top gated graphene FE-FET seen in Fig. 1(d) for different V_{GS} scan rates (dV_{GS}/dt). For each dV_{GS}/dt, V_{GS} was scanned in a closed loop from −25 V → +25 V → −25 V while V_{DS} was fixed at 100 mV. At the end of each scan, V_{GS} was held constant at −25 V for 300 s in order for the current to recover its original value before the next scan rate was selected, and the process was repeated. The red arrows show the current response for dV_{GS}/dt = 1000 mV/s during the scan and indicate the general direction of the current response for other scan rates. As V_{GS} is varied from −25 V → +25 V, the current passes through a minimum in the first quadrant, corresponding to the charge neutrality point (CNP-1) in graphene.[20] As V_{GS} varies from +25 V → −25 V, the currents retain their initial value for a range of V_{GS} due to polarization of the

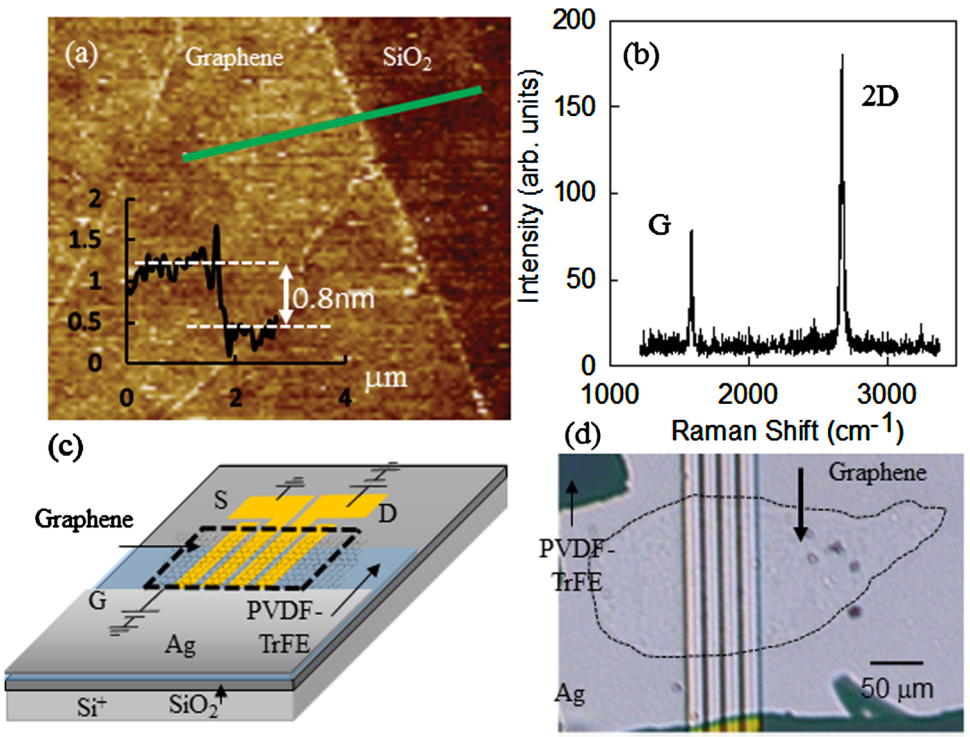

FIG. 1. (a) AFM image of CVD graphene used in this work, with an edge height profile measured along the green line. (b) Raman spectrum of CVD graphene used in this work. (c) Schematic labeled diagram of the device showing the external electrical connections. (d) Optical microscope image of the dashed portion seen in (c) and is the actual device investigated. The dashed curve shows the outline of the graphene film.

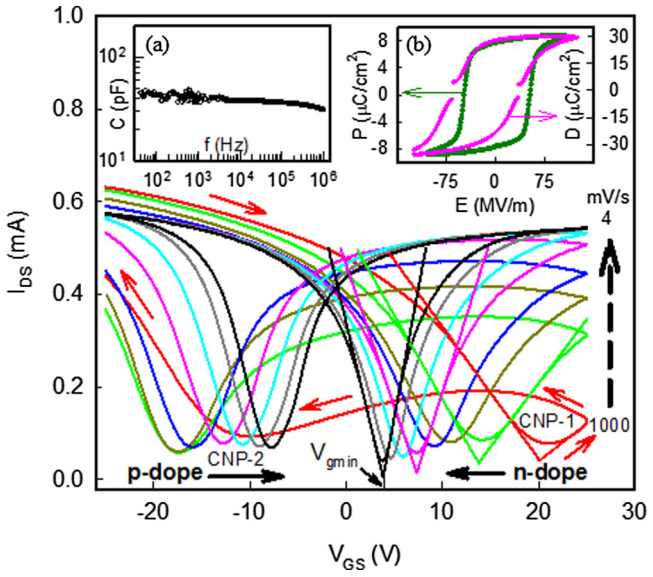

FIG. 2. I_{DS} vs V_{GS} of the graphene FE-FET for the following V_{GS} scan rates indicated by the dashed arrow in mV/s: 1000 (red), 400 (green), 200 (dark yellow), 100 (blue), 40 (pink), 20 (cyan), 10 (dark gray), and 4 (black). V_{DS} was fixed at 100 mV. The red arrows show the general direction of the current response as V_{GS} is scanned. The straight lines are fits to the linear portion of the data and are shown for a few selected scan rates. Insets: (a) Frequency dependence of the FE gate capacitance measured between the G and D terminals of the FE-FET. (b) Electric field dependence of the polarization (P) of a thin film PVDF–TrFE capacitor (dark green) and the extracted electric displacement (D) for the graphene FE-FET, taken at a scan rate of 40 mV/s (pink). The discontinuity is due to the polarization reversal in the FE gate at the charge neutrality points. V_{gmin} is the voltage at the charge neutrality point. CNP-1 and CNP-2 represent the charge neutrality points in the first and second quadrant, respectively.

FE gate. When V_{GS} is made more negative, the current decreases, passing through a minimum again in the second quadrant that also corresponds to a charge neutrality point (CNP-2). The observed hysteresis and double minima are consistent with other reports on graphene based FE-FETs and are related to the polarization of the FE gate.[20–23] In crossing CNP-1 from left to right, the polarization flips direction from ↑ to ↓ and reverses direction in crossing CNP-2 from right to left.[21] This general trend in the current is observed independently of how V_{GS} is scanned (i.e., −25 V → +25 → −25 V or +25 V → −25 V → +25 V or 0 → +25 V → −25 V → 0 V) (Figs. S3 and S4 in the supplementary material). The current variation away from the CNPs is governed by charge scattering[10] (long and short range) and also by the polarization of the FE gate.[20] The main features observed in Fig. 2 as the scan rate is lowered are (i) CNP-1 shifts to the left (*n*-type doping) and CNP-2 shifts to the right (*p*-type doping), (ii) the electron and hole mobility increases and the width (ΔV_{gmin}) near both CNPs gets smaller, (iii) I_{DS} vs V_{GS} curves stay linear for a smaller range of V_{GS} values, (iv) the minimum current value (at the CNP) increases initially and then decreases, and (*v*) I_{DS} measured at V_{GS} = +25 V increases non-linearly.

To understand these features, the electrical properties of the FE gate were investigated. Inset (a) in Fig. 2 shows the frequency dependence of the FE gate capacitance measured between the G and D terminals of the device. At high frequencies, the capacitance decreases due to the inertia of the dipoles not being able to follow the rapidly changing electric field.[19] At low frequency, the capacitance is seen to approach 45 pF yielding a specific capacitance (C_i) of 80 nF/cm^2. For comparison, the specific capacitance of a 150 nm thick SiO_2 film is ∼20 nF/cm^2.[24] In a separate thin film (700 nm) PVDF–TrFE capacitor, spontaneous polarization was measured at 1 Hz and plotted vs E in inset (b) in Fig. 2. The hysteresis curve confirms the two state (↑↓) polarization of the FE gate with saturation polarization (∼9 μC/cm^2) and coercive field (E_c ∼ 50 MV/m) values consistent with previous reports.[20,21,25] The PVDF–TrFE film thickness measured with the profilometer for the capacitor and the FE-FET (away from the Au electrodes) was ∼700 nm. The CNP in graphene was found to lie near the FE gate coercive field.[20,21] Using the coercive field of 50 MV/m, we estimate the film thickness between the S/D electrodes in the FE-FET to be ∼200 nm (see the supplementary material). The polarizable [$\mathbf{P}(V_{GS})$] component of the electric displacement field ($\mathbf{D} = \varepsilon\mathbf{E} + \mathbf{P}$) in the FE gate is responsible for the observed hysteresis,[21] where ε is the dielectric permittivity of PVDF–TrFE and **E** the applied electric field. The continuity of D at the graphene/FE gate interface yields the relationship $D = G/\mu$,[21] where G is the conductance and μ is the mobility. Choosing, for example, the data corresponding to dV_{GS}/dt = 40 mV/s shown in Fig. 2, D is calculated and plotted in the inset (b) in Fig. 2. The mobility $\left(\mu = \frac{g_m L}{W C_i V_{DS}}\right)$ (see the inset

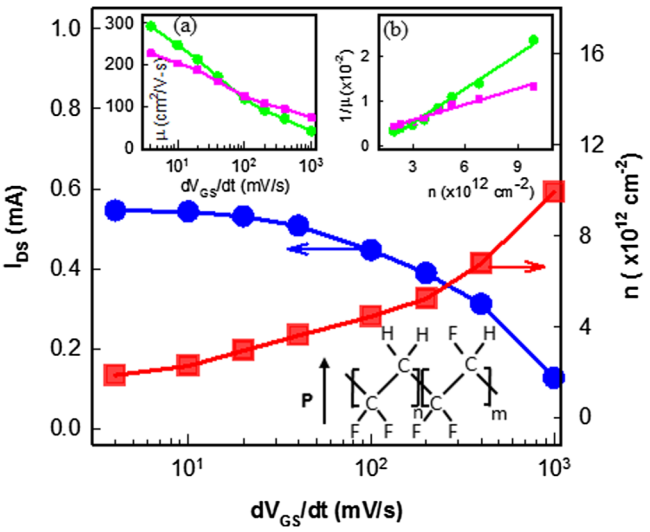

FIG. 3. I_{DS} measured at V_{GS} = + 25 V (taken from Fig. 2) vs dV_{GS}/dt (blue color symbol). Dopant concentration (n) as a function of dV_{GS}/dt (red color symbol). Lower inset: PVDF–TrFE chemical structure with the polarization (**P**) pointing up. Inset (a): Electron (green color symbol) and hole (pink color symbol) mobilities as a function of dV_{GS}/dt. Inset (b): $1/\mu$ vs *n* for electrons (green color symbol) and holes (pink color symbol). The straight lines are linear fits to the data. The lines in main figure and inset (a) are guides to the eye.

in Fig. 3) was calculated from the device trans-conductance $\left(g_m = \frac{dI_{DS}}{dV_{GS}}\right)$. This parameter ($g_m$) was obtained from the slope of the straight line (straight lines) fits to the linear portion of the data shown in Fig. 2. The similarity between **P** and **D** curves strongly suggests that the observed hysteresis in the FE-FET is correlated with the polarization of the FE gate. A discontinuity is observed in the D vs E plot and occurs at the CNPs in graphene, while a slight shift to the left is due to the fact that the position of the two CNPs in Fig. 2 is not symmetric about $V_{GS} = 0$ V. The majority carriers in graphene are electrons for $V_{gmin(CNP\text{-}1)} < V_{GS} < +25$ V and holes for -25 V $< V_{GS} < V_{gmin(CNP\text{-}2)}$. For V_{GS} values in other intervals, the majority carriers could be electrons or holes depending on the doping contribution from the linear (ε**E**) and hysteretic part [**P**(V_{GS})] of **D**. The maximum currents in Fig. 2 depend on the polarization of the FE gate, which is dependent on dV_{GS}/dt.

Figure 3 and the insets in the figure show the variation of some device parameters extracted from the data in the first quadrant in Fig. 2, as a function of dV_{GS}/dt. The chemical structure of the FE gate when polarized ↑ is displayed in the lower inset. The FE gate polarization is postulated to control doping in graphene. We have previously shown that for high dV_{GS}/dt, the coercive field increases and the polarization does not reach true saturation as FE domains in the copolymer have insufficient time to grow.[26] At slower dV_{GS}/dt, however, FE domains are able to follow the polarizing field achieving higher growth and then coalesce resulting in higher saturation at lower coercive fields. At $V_{GS} = +25$ V, the channel current increases proportionately to the FE gate polarization, which depends on dV_{GS}/dt as seen in Fig. 2. This current is plotted as a function of dV_{GS}/dt in Fig. 3 and shows a non-linear increase, reaching a saturation value of 0.55 mA at a slower dV_{GS}/dt due to the saturated polarization of the FE gate. Figure 3 also shows a plot of the dopant concentration $\left(n = \frac{C_i V_{gmin}}{e}\right)$ that decreases non-linearly for smaller dV_{GS}/dt. As dV_{GS}/dt is lowered, the relative shift of CNP-1 toward the left indicates *n*-type doping, and the change in *n*-type dopant concentration reaches 8×10^{12} cm^{-2}. Theory predicts that the impurity charge concentration is inversely proportional to the mobility of electrons and holes,[10] and our results are consistent. The upper right inset in Fig. 3 shows a plot of $1/\mu$ vs n for electrons and holes, where the slopes of the best fit lines are 2.5×10^{-15} V s for electrons and 1.2×10^{-15} V s for holes. It is important to observe that both the current at $V_{GS} = +25$ V and n tend to saturate as dV_{GS}/dt is lowered. This is because the FE gate cannot be polarized beyond the saturation limit. It was shown that charged impurities influence the quantum capacitance[27] in graphene and that it depends on V_{GS}.[28] Graphene doping could, therefore, be affected by this capacitance especially near the CNP.[29] However, the large dielectric permittivity (10) and thickness (200 nm) of the FE gate together with large values of V_{gmin} (>1 V) make quantum capacitance effects negligible.[30] Figure 4 shows the I_{DS} vs V_{GS} curve where V_{GS} is scanned from -25 V → $+25$ V → -25 V at a fixed dV_{GS}/dt, and repeated as dV_{GS}/dt is lowered in steps from 1000 mV/s to 10 mV/s. This experiment is then repeated again as dV_{GS}/dt is increased from 10 mV/s to 1000 mV/s in the same steps after each scan. The results are similar to those observed in Fig. 2. Figure 4, however,

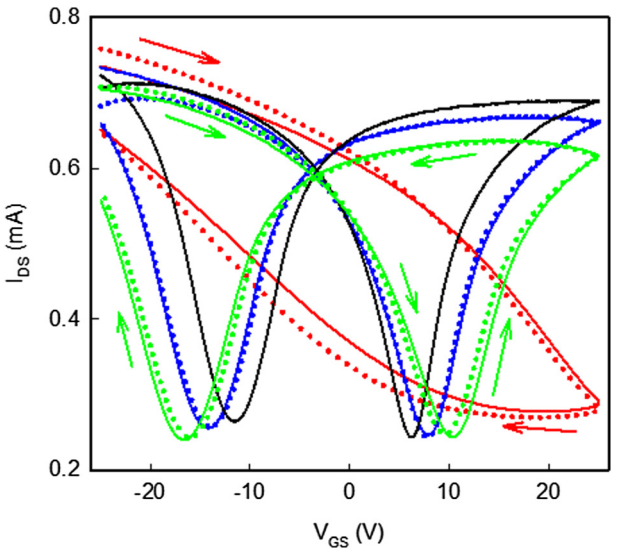

FIG. 4. I_{DS} vs V_{GS} of the graphene FE-FET for different dV_{GS}/dt. V_{DS} was fixed at 100 mV and V_{GS} was swept as follows for each dV_{GS}/dt: -25 V → $+25$ V → -25 V. The experiment started with a scan rate of 1000 mV/s, and the rate stepped down like in Fig. 2 to 10 mV/s (dotted lines) and then stepped back up to 1000 mV/s (continuous lines). Only data for the 10 mV/s (black), 20 mV/s (blue), 40 mV/s (green), and 1000 mV/s (red) are shown. The arrows indicate the direction of current response. The curves trace over each other implying that the doping process is non-destructive and is reversible.

shows that the curves for identical dV_{GS}/dt trace over each other, retaining a similar V_{gmin} at the CNP and mobility values, and confirms that the doping process is non-destructive and reversible. Analyzing the data in the second quadrant of Fig. 2 for *p*-type doping yields qualitatively similar results. The stability of the device was tested and found to operate normally even after storage in a desiccator for a month (Fig. S5 in the supplementary material).

Figure 5(a) illustrates an easy way to interpret our results. During growth and device fabrication, charged impurities of both signs are unintentionally adsorbed on to the graphene surface as shown in the figure. When $V_{GS} = -25$ V (and $V_{DS} = 100$ mV), the current in graphene reaches its maximum value due to the saturated polarization ↑ of the FE gate, as confirmed by inset (b) in Fig. 2 for slow scan rates. Subsequently, a negative surface (bound) charge in the FE gate at the interface with graphene is established due to individual dipole orientation (ovals). This charge electrostatically *p*-dopes graphene and also compensates and neutralizes positive impurity charge as seen in Fig. 5(a). The compensation leaves an excess negative impurity charge on graphene, which in turn *p*-dopes it even further. When $V_{GS} = +25$ V, the polarization points ↓ and the opposite charge dynamics occur. Thus, as V_{GS} is scanned from -25 V to $+25$ V, the FE gate polarization in the ↑ direction decreases, reaching a minimum, and then increases in the ↓ direction. During this process, the negative surface (bound) charge density at the FE gate/graphene interface decreases, changes sign, and then increases. This results in a decrease of electrostatic *p*-doping in graphene and the compensation of the positive

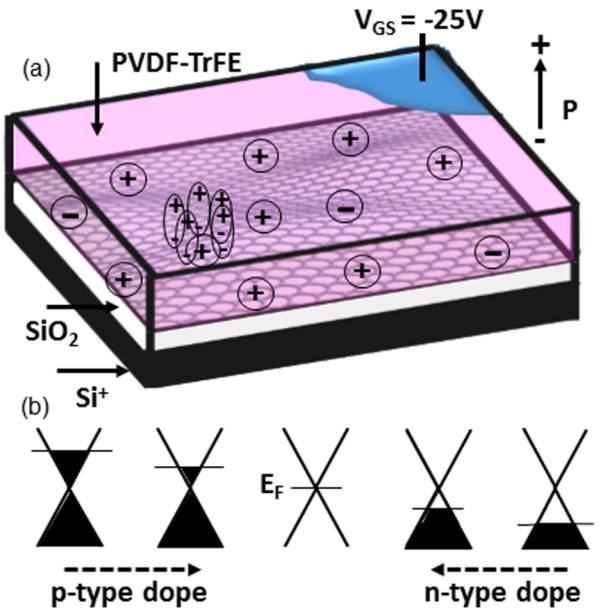

FIG. 5. (a) Schematic model illustrating polarization assisted doping in graphene. The S and D electrodes are omitted for clarity. Impurity charges on the graphene surface are compensated and neutralized by the polarization of PVDF–TrFE. The polarization **P** points up (down) when V_{GS} is negative (positive). (b) Band diagram of graphene showing how the Fermi energy (E_F) increases for *n*-type doping and decreases for *p*-type doping as indicated by the dashed arrows.

impurity charges, and in an increase in the electrostatic *n*-doping and compensation of negative impurity charges. As V_{GS} is scanned from $-25\,V \rightarrow +25\,V$, CNP-1 shifts to the left as dV_{GS}/dt is lowered. The reason is as follows: at the start of each scan, the FE gate is polarized ↑ at $V_{GS} = -25\,V$. If dV_{GS}/dt is high for, e.g., 1000 mV/s, the polarization is not able to follow the changing electric field and stays "frozen" while E_c increases, this means that a large portion of positive impurity charges stay compensated even as V_{GS} approaches +25 V, and the uncompensated negative charge maintains *p*-doped graphene. Thus, CNP-1 is to the far right on the V_{GS} axis. When dV_{GS}/dt is lowered, E_c decreases; the polarization is able to follow the changing electric field and decreases accordingly as V_{GS} approaches CNP-1. Hence, the number of compensated positive impurity charges is lowered. These newly exposed positive impurity charges, in turn, compensate for and neutralize an equivalent number of negative impurity charges. Fewer uncompensated negative impurity charges now imply that *p*-doping in graphene is weakened and CNP-1 moves to the left as dV_{GS}/dt is lowered further. It also shows why the dopant concentration decreases as dV_{GS}/dt is lowered. As V_{GS} is scanned back from +25 V to −25 V, equivalent but opposite charge dynamics shifts CNP-2 to the right as dV_{GS}/dt is lowered. Thus, the two CNPs move toward each other as dV_{GS}/dt is lowered. A similar effect was observed in back gated graphene using a surface aqueous solution with increasing ionic concentration.[31]

When V_{GS} is changed from $-25\,V \rightarrow +25\,V$ at 1000 mV/s, for example, CNP-1 is located far to the right on the V_{GS} axis as a large fraction of the positive impurity charges are compensated. As V_{GS} increases beyond CNP-1, the polarization switches direction, but the bulk polarization is not able to saturate (red curve in Fig. 2) since the gate voltage has reversed its scan direction. The graphene channel is, therefore, weakly *n*-doped in this case, and few negative impurity charges are compensated. Thus, when V_{GS} is scanned back from $+25\,V \rightarrow -25\,V$, the hysteretic effect of the polarization [$\mathbf{P}(V_{GS})$] diminishes quickly, the linear portion ($\varepsilon\mathbf{E}$) of $\mathbf{D}$ then dopes graphene with opposite polarity,[21] and the polarization switches direction once again. This results in a broad ill-defined CNP-2 (red curve in Fig. 2). At slower scan rates, as V_{GS} increases beyond CNP-1, the polarization gets stronger, and the current becomes larger. Hence, during the reverse scan from +25 V to −25 V, we observe a sharper CNP-2. Figure 5(b) illustrates the doping process via shifts of the Fermi energy (E_F) toward higher values for *n*-type doping and toward lower values for *p*-type doping. The validity of our model is strengthened by the observed mobility dependence on dV_{GS}/dt (upper left inset to Fig. 3). The mobility increases but does not appear to saturate as dV_{GS}/dt is lowered, even as the dopant carrier concentration saturates to a lower value. One reason is the efficient compensation of the charged impurity. Lowering dV_{GS}/dt allows polymer chain readjustment, resulting in controlled polarization growth and an increasingly uniform surface (bound) charge. The associated charge rearrangement efficiently compensates adsorbed impurity charges of one sign and homogeneously redistributes the decreasing number of uncompensated charges of the opposite sign on the graphene surface. The result is increased mobility for both species of charges and a narrowing of ΔV_{gmin} as observed in Fig. 2 as dV_{GS}/dt is lowered. Thus, we propose that the doping process is initiated by the polarization and subsequent compensation of impurity charges. The hermitic seal provided by the FE gate traps the impurity charges, contributing to the reversibility of the doping process. It also protects the graphene layer and prevents external charges from reaching it, confirming that the doping is via impurity charges adsorbed on the graphene surface. Gate modulated charge carriers using ferroelectrics were successfully tested in MoS_2 and WSe_2 films.[15,16] Lateral charge control in these 2D materials resulted in p–n or Schottky diodes and demonstrate a new way for fabricating continuous junctions of varying charge densities and charge types.

IV. CONCLUSIONS

In conclusion, we show that doping in graphene can also be achieved via compensating adsorbed impurity charges using the polarization of a FE gate. No external charges are added in this process. Furthermore, graphene can be doped with either charge polarity by controlling the polarization and its direction. Compensating one type of charge impurity results in doping due to the uncompensated charge of the opposite type. A change in the *n*-type dopant concentration of $8 \times 10^{12}\,cm^{-2}$ was observed, with the electron mobility changing by 650%. The doping process is reversible and does not damage graphene. The possibility of selectively doping graphene without introducing hard junctions makes this technique attractive for integrating multiple devices on a continuous film.

SUPPLEMENTARY MATERIAL

See the supplementary material for more experimental details.

ACKNOWLEDGMENTS

This work was supported by the National Science Foundation (NSF) under Grant Nos. DMR-PREM-1523463 and DMR-RUI-1800262. M.-Q.Z. and A.T.C.J. acknowledge support from the NSF through Nos. MRSEC DMR-1720530 and EAGER 1838412. M.D. and P.M.D. acknowledge funding from NSF (MRSEC) Nos. DMR-1720530, NSF EFRI 2-DARE 1542707, NSF EAGER 1838456, NSF DMR 1905045, and NIH R21 HG010536.

REFERENCES

[1]A. K. Geim and K. S. Novoselov, Nat. Mater. **6**, 183 (2007).
[2]K. S. Novoselov, A. K. Geim, S. V. Morozov, D. Jiang, Y. Zhang, S. V. Dubonos, I. V. Grigorieva, and A. A. Firsov, Science **306**, 666 (2004).
[3]K. S. Novoselov, A. K. Geim, S. V. Morozov, D. Jiang, M. I. Katnelson, I. V. Grigorieva, S. V. Dubonos, and A. A. Firsov, Nature **438**, 197 (2005).
[4]A. H. Castro Neto, F. Guinea, N. M. R. Peres, K. S. Novoselov, and A. K. Geim, Rev. Mod. Phys. **81**, 109 (2009).
[5]R. Lv Q. Li *et al.*, Sci. Rep. **2**, 586 (2012).
[6]Z. Jin, J. Yao, C. Kittrell, and J. M. Tour, ACS Nano **5**, 4112 (2011).
[7]W. Chen, D. Qi, X. Gao, and A. T. S. Wee, Prog. Surf. Sci. **84**, 279 (2009).
[8]F. Schedin, A. K. Geim, S. V. Morozov, E. W. Hill, M. I. Katsnelson, and K. S. Novoselov, Nat. Mater. **6**, 652 (2007).
[9]T. O. Wehling, K. S. Novoselov, S. V. Morozov, E. E. Vdovin, M. I. Katnelson, A. K. Geum, and A. I. Lichtenstein, Nano Lett. **8**, 173 (2008).
[10]J. H. Chen, C. Jang, S. Adam, M. S. Fuhrer, E. D. Williams, and M. Ishigami, Nat. Phys. **4**, 377 (2008).
[11]L. S. Panchokarla *et al.*, Adv. Mater. **21**, 4726 (2009).
[12]X. R. Wang *et al.*, Science **324**, 768 (2009).
[13]X. Wang, P. Wang, J. Wang *et al.*, Adv. Mater. **27**, 6575 (2015).
[14]H. S. Lee, S. W. Min, M. K. Park, Y. T. Lee, P. J. Jeon, J. H. Kim, S. Ryu, and S. Im, Small **8**, 3111 (2012).
[15]Z. Xiao, J. Song, D. K. Ferry, S. Ducharme, and X. Hong, Phys. Rev. Lett. **118**, 236801 (2017).
[16]J. W. Chen, S. T. Lo, S. C. Ho *et al.*, Nat. Commun. **9**, 1–7 (2018).
[17]Z. Gao, H. Kang, C. H. Naylor *et al.*, ACS Appl. Mater. Interfaces **8**, 27546 (2016).
[18]A. C. Ferrari, J. C. Meyer, V. Scardaci *et al.*, Phys. Rev. Lett. **97**, 187401 (2006).
[19]T. Furukawa, Y. Tajitsu, X. Zhang, and G. E. Johnson, Ferroelectrics **135**, 401 (1992).
[20]X. Wang, Y. Chen, G. Wu, J. Wang *et al.*, Nanotechnology **29**, 134002 (2018).
[21]Y. Zheng, G. X. Ni, C. T. Toh, M. G. Zeng, S. T. Chen, K. Yao, and B. Ozyilmaz, Appl. Phys. Lett. **94**, 163505 (2009).
[22]Y. Zheng, G. X. Ni, C. T. Toh, K. Yao, and B. Ozyilmaz, Phys. Rev. Lett. **105**, 166602 (2010).
[23]Y. Zheng, G. X. Ni, S. Bae *et al.*, Europhys. Lett. **93**, 17002 (2011).
[24]J. H. Cho, J. Lee, Y. He, B. S. Kim, T. P. Lodge, and C. D. Frisbie, Adv. Mater. **20**, 686 (2008).
[25]N. Meng, R. Mao, W. Tu, X. Zhu, R. M. Wilson, E. Bilotti, and M. J. Reece, Polymer **100**, 69 (2016).
[26]N. J. Pinto, L. M. Rijos, M. Q. Zhao, W. M. Parkin, and A. T. Charlie Johnson, Ferroelectrics **550**, 1 (2019).
[27]J. Xia, F. Chen, J. Li, and N. Tao, Nat. Nanotechnol. **4**, 505 (2009).
[28]T. Fang, A. Konar, H. Xing, and D. Jena, Appl. Phys. Lett. **91**, 092109 (2007).
[29]S. Droscher, P. Roulleau, F. Molitor, P. Studerus, C. Stampler, K. Ensslin, and T. Ihn, Appl. Phys. Lett. **96**, 152104 (2010).
[30]S. Das Sarma, S. Adam, E. H. Hwang, and E. Rossi, Rev. Mod. Phys. **83**, 407 (2011).
[31]F. Chen, J. Xia, and N. Tao, Nano Lett. **9**, 1621 (2009).